

# Chapter 9

## Design of Geocell-Reinforced Pavement Bases



Sireesh Saride and Vijay Kumar Rayabharapu

**Abstract** This chapter deals with the design of geocell-reinforced pavement bases which includes the evaluation of the influence of geocell reinforcement on granular aggregate base courses overlying weak clayey soil subgrades. A series of large-scale model tests under static and repeated loading was performed to obtain the influence of geocell-reinforcement, with and without basal geogrid, on the structural capacity of the base layer. An improved stiffness and resilient behavior of the granular base layer was obtained with the geocell-reinforcement in lieu of an additional lateral confinement provided to the granular material. The normalized contact pressure at the interface of the granular base and weak subgrade layers was observed to be well minimal. From the pilot field studies, it was also observed that about 62% of the applied pressure has been absorbed by the reinforced granular base layer and transmitted about 38% to the underlying weak subgrade layer. Finally, two design methodologies, viz traffic benefit ratio (TBR) approach and layer coefficient ratio (LCR) approach, are discussed in this chapter along with the examples from the inputs of the large-scale testing.

**Keywords** Base course · Geocell reinforcement · Contact pressure · Settlements · Traffic benefit ratio · Layer coefficient ratio

### 9.1 Introduction and Background

A variety of soil subgrades ranging from dense to very loose and stiff to very weak are encountered around the world. Stabilizing such weak subgrades is inevitable as availability of good construction sites is limited and at times, they are unavoidable. For the past few decades, the use of geosynthetics has been gaining advantages

---

S. Saride (✉)  
Indian Institute of Technology, Hyderabad, Telangana, India  
e-mail: [sireesh@ce.iith.ac.in](mailto:sireesh@ce.iith.ac.in)

V. K. Rayabharapu  
BV Raju Institute of Technology, Narsapur, Telangana, India  
e-mail: [vkraya@gmail.com](mailto:vkraya@gmail.com)

© Springer Nature Singapore Pte Ltd. 2020  
T. G. Sitharam et al. (eds.), *Geocells*, Springer Transactions  
in Civil and Environmental Engineering,  
[https://doi.org/10.1007/978-981-15-6095-8\\_9](https://doi.org/10.1007/978-981-15-6095-8_9)

over the other improvement methods, especially in the pavement industry. Recently, the application of geocells in pavement layers has been showing high-performance improvement as it can provide additional lateral confinement to the infill material over and above the stabilization functions provided by conventional geosynthetics. Several research studies have shown in the past that the geocell reinforcement is effective when a granular infill is used over weak subgrades (Dash et al. 2003; Rajagopal et al. 2012; Pokharel et al. 2011; Perkins and Ismeik 1997; Latha et al. 2010) under monotonic loading conditions. Studies were performed on varieties of geosynthetics such as geotextiles and grids under cyclic loading under a moving single wheel system in an outdoor test track (Barker 1987; Haas et al. 1988; Barksdale et al. 1989; Collin et al. 1996). These studies reported a traffic benefit ratio (TBR) of 2.8 and 2.3 when a moving single wheel applying a pressure of 500 kPa. Pokharel (2010) demonstrated the behavior of geocell-reinforced granular bases over clay subgrades under cyclic loading. However, not much information is reported in the literature on repeated load tests on pavement sections reinforced with geocells with extensive instrumentation.

Besides, field performance studies on geocell-reinforced pavements are very few. Field tests on full-scale road sections have been conducted by Perkins and Ismeik (1997) and compared the results from nine test track sections including indoor and outdoor using a two-axle, dual-wheel truck to load the pavement which resulted in significant improvement with the geosynthetic reinforcement. Latha et al. (2010) performed field studies on unpaved roads reinforced with a variety of geosynthetics including geocells and reported an increase in load-carrying capacity with a reduction in rut depth. However, the behavior of geocells in the actual field conditions under cyclic/repeated loading is not understood completely to derive the design parameters.

The reinforcing effect of geosynthetics in pavements is usually assessed through two parameters, i.e., traffic benefit ratio (TBR) (AASHTO 2009) and layer coefficient ratio (LCR). The LCR is defined as the ratio of the layer coefficient of a reinforced section to reach a given rutting depth to the ratio of layer coefficient of an unreinforced section with the same geometry and material constituents that reaches the same rutting depth. The LCR value can be determined in the laboratory on a large-scale test through modulus improvement factor, MIF (Giroud and Han 2013) as follows.

$$\text{LCR} = \frac{0.249 \log 10 \left( \text{MIF} * \frac{M_{\text{rbc}}}{0.0069} \right) - 0.977}{0.249 \log 10 \left( \frac{M_{\text{rbc}}}{0.0069} \right) - 0.977} \quad (9.1)$$

where

MIF = Modulus improvement factor

$M_{\text{rbc}}$  = Resilient modulus of base course in MPa.

The American Association of State Highways and Transportation Officials (AASHTO) proposed a flexible pavement design based on overall structural number (SN) (AASHTO 1993) as follows.

$$\text{SN} = a_1 D_1 + a_2 D_2 m_2 + a_3 D_3 m_3 \quad (9.2)$$

where  $SN$  = Structural number depends on the pavement layer thicknesses ( $D$ ), layer coefficients ( $a$ ), and drainage coefficients ( $m$ ).

In order to design the reinforced pavement section, the traffic benefit ratio (TBR) can be used. The effect of geocell reinforcement is quantified in terms of equivalent structural number by considering traffic to be catered by the pavement and TBR that can be obtained with selected geocell. The equivalent structural number of geocell is then used to reduce the unreinforced pavement layer thicknesses to the extent of the reinforcement effect.

In this chapter, the behaviors of geocell, with/without basal layers overlying weak clay subgrades subjected to static and repeated loading, are discussed through extensive experimental studies and field studies. At this point, the guidelines available to design pavements incorporating geosynthetics are in the nascent stage. The design methodologies presented in IRC SP 59 (2019) are discussed.

## 9.2 Experimental Studies

Before conducting actual field studies on geocell-reinforced granular bases, extensive laboratory studies were performed to ascertain the efficacy of the geocell reinforcement in pavements. For the laboratory experimental program, clayey soil was selected to replicate a very weak subgrade. It was envisioned that the effect of geocells can be visualized over weak subgrades. Conventional granular aggregate material (wet mix macadam, WMM) was adopted to use as an infill material, and a geocell mattress made of high-density polypropylene (HDPE) material was selected.

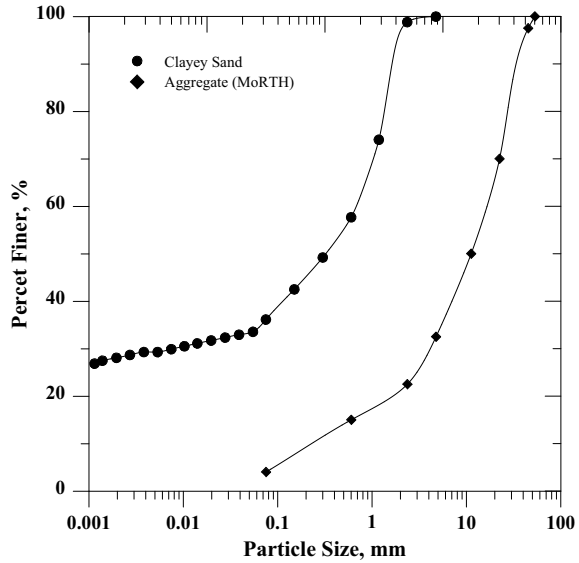
### 9.2.1 Material Properties

#### Clayey Soil

The material used for the preparation of subgrade is a natural lateritic sandy clay obtained from an open excavation on the campus of the Indian Institute of Technology, Hyderabad. Wet sieve analysis was performed to determine the particle size distribution of the soil. Figure 9.1 shows the particle size distribution curve of clayey soil, which had a 40% fines fraction smaller than  $75 \mu$  sieve size. The specific gravity of the soil is 2.68.

The maximum unit weight of  $20.5 \text{ kN/m}^3$  and 14% optimum moisture content are obtained for the soil. Liquid limit and plastic limits are found to be 46% and 21%, respectively. As per the USCS, the soil can be classified as clayey sand (SC). To know the shear strength parameters of the soil, compacted at wet unit weight, standard triaxial compression tests were conducted. A friction angle of  $14^\circ$  and a cohesion of 14 kPa were observed from the triaxial tests.

**Fig. 9.1** Grain size distribution of clayey soil and granular base material



**Granular Aggregate**

The granular base infill material was obtained from a local suburban quarry site near the campus. The aggregate material has been chosen according to the Ministry of Road transport and Highways (MORTH) specification for the pavement base layers. The particle size distribution of aggregates is obtained by performing dry sieve analysis and the corresponding gradation curve of aggregates as shown in Fig. 9.1.

**Geocell**

A high-density polyethylene (HDPE) geocell material was selected for the study. Various properties of the geocells like the material composition, density, weld spacing, weld depth, and seam strength are given in Table 9.1.

Test Setup

**Table 9.1** Properties of geocell material

Properties	Values
Density, g/cm <sup>3</sup>	0.935–0.965
Weld spacing (mm)	356
Cell depth (mm)	200
Min. seam strength (N)	2800
Cell size (±10%) (mm)	259 × 224
Cell area (±4%)	290

Figure 9.2 shows the experimental facility consisting of a test tank of size 1.0 m × 1.0 m × 1.0 m, a double-acting linear actuator to apply traffic loads a reaction frame to support the actuator, and a controller and recording system used in the current study. The clayey soil subgrade was first prepared in a test tank. A fairly uniform average bulk unit weight of 20.5 kN/m<sup>3</sup> at 20% placement water content was consistently maintained throughout the test program. In order to verify the uniformity of the testbed, undisturbed core samples were collected from different locations to determine the in situ unit weight and moisture contents. The data shows that the bed properties are fairly maintained with an error margin of 2%. At this compacted condition, the subgrade has an undrained strength of 10 kPa determined from a series of unconfined compressive strength tests. Once the weak subgrade was prepared up to the required grade in the test tank, granular base layers were prepared on the weak subgrade with or without geocell reinforcement.

To prepare the unreinforced testbed, the granular base layer was placed in the test tank and compacted in 50 mm thick layers till the desired height was reached. For each layer, the required amount of aggregate to produce a desired bulk unit weight 23 kN/m<sup>3</sup> was weighed out and placed in the test box making use of a metal scoop. The granular base was then gently leveled and compacted using a 5.0 kg drop hammer to a pre-calibrated number of blows to achieve the required density. A similar procedure was used to compact the base material inside the geocell pockets as well. Once the

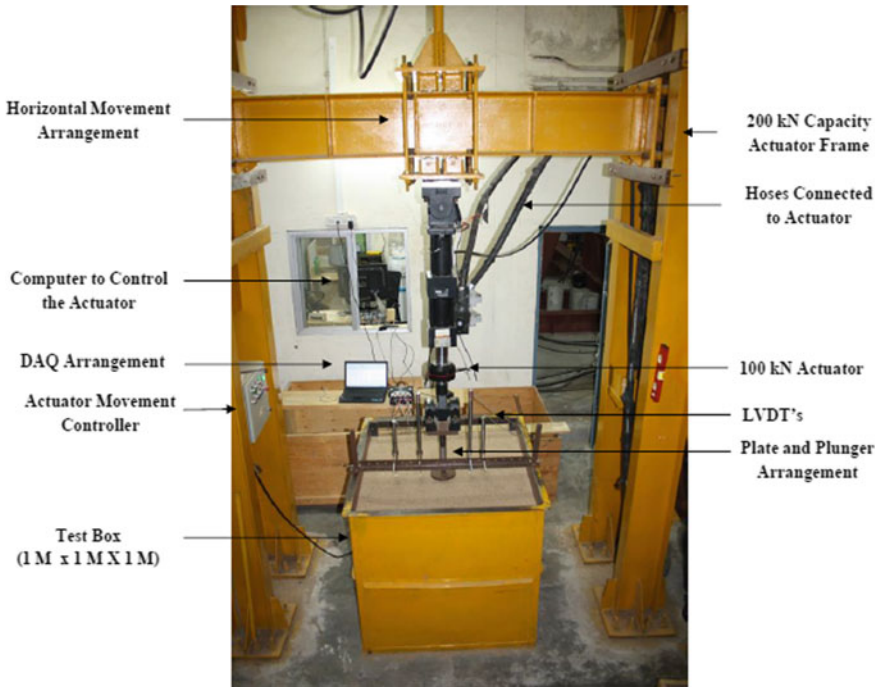


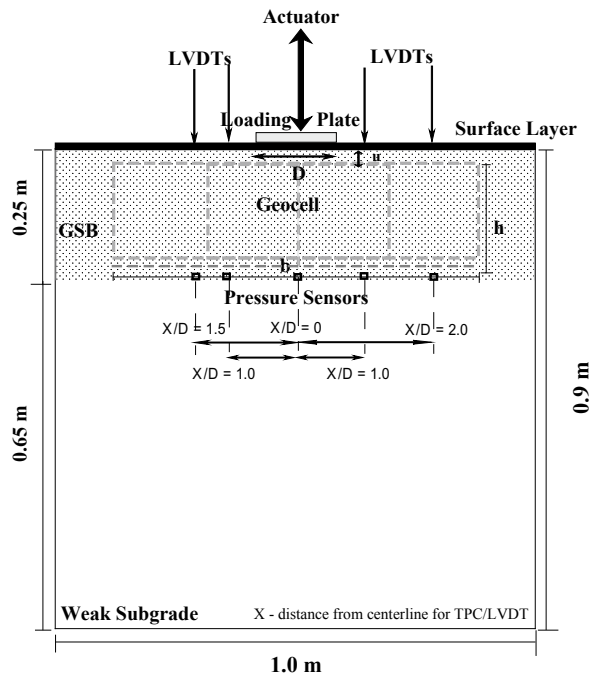
Fig. 9.2 Experimental facility used in the current study

final grade was reached, a rigid thin steel plate of 150 mm diameter ( $D$ ) and 15 mm thickness was concentrically placed to apply an appropriate repeated traffic loading. Loading was given by graphical user interfaced MTS<sup>®</sup> multi-purpose test software with the help of hydraulic power unit (HPU), hydraulic service manifold (HSM), and sophisticated double-acting linear dynamic 100 kN capacity actuator which is attached to a 3.5 m high, 200 kN capacity reaction frame as shown in Fig. 9.2.

Normal contact pressure developed on the subgrade at various points was measured using strain gauge type earth pressure cells. Five numbers of total earth pressure cells (TPC) with one 1000 kPa, two of 500 kPa, and two of 200 kPa capacities were used. The 1000 kPa capacity pressure cell was placed at the centerline of the loading plate, and 500 and 200 kPa TPCs were kept at a distance of  $1.0D$ ,  $1.5D$ , and  $2D$  from the centerline of the loading plate on either side of the plate, respectively, as shown in test schematic Fig. 9.3. In the case of unreinforced sections, the TPCs were placed at the interface. The pressures were measured from a DAQ system, which directly shows the pressure through the computer display connected to it.

In addition, the vertical deformations (i.e., settlement of the loading plate and surface heave/settlement of the bed) were measured using linear variable differential transformers (LVDT's). The LVDT's were of 50 mm and 100 mm travel with 0.001 accuracy. Small plates of size 20 mm length  $\times$  20 mm width  $\times$  4 mm thickness made of perspex sheet were placed on the compacted granular surface at required locations to support the LVDTs, where the surface deformations are to be measured.

**Fig. 9.3** Schematic test setup of geocell-reinforced clayey soil subgrade



The deformations (heave/settlement) of the soil surface on either side of the footing were measured by dial gauges placed at a distance of  $1.0D$ ,  $1.5D$ , and  $2.0D$  from the centerline on either side of the loading plate. The placement position of these LVDT’s was decided based on the findings reported by Chummar (1972) that the heaving on soil surface extends up to a distance of about twice the width of the footing from the edge of the footing with a maximum heaving occurring at around  $1.5D$  from the center of the footing. A close-up view of the LVDT’s used in the test setup can also be seen in Figs. 9.2 and 9.3.

### 9.3 Experimental Program

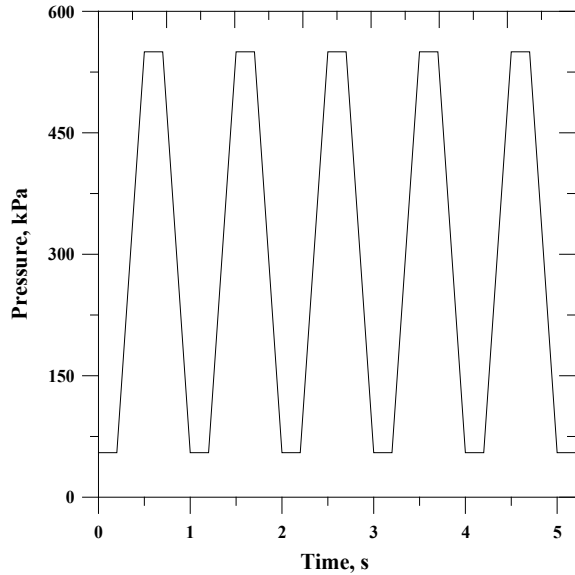
Figure 9.3 shows the schematic of geocell-reinforced granular base over weak clayey subgrades used in the study. A series of monotonic and repeated load tests were conducted on geocell-reinforced granular base over weak clayey subgrades and along with the placement of additional basal geogrid as summarized in Table 9.2. All the other optimum geocell geometric parameters were maintained from Saride et al. (2015) while subgrade conditions are kept constant. The objective of the experimental program is to understand how much rut depth can be controlled by using geocells in the base layer as well as to quantify the benefit in terms of traffic.

In a static load test, the load was applied in displacement mode at a rate of 0.5 mm/min. In a repeated load test, the load was applied on to the plate using a

**Table 9.2** Details of testing program

Test description/Nomenclature	Constant parameters
Unreinforced granular base over clayey soil subgrade (UGC)	$\gamma_d = 23.1 \text{ kN/m}^3$ $C_u = 10 \text{ kPa}$ $H/D = 1.67$
Unreinforced granular base over clayey soil subgrade and surface layer (U G C SL)	Surface layer $\gamma_d = 23.1 \text{ kN/m}^3$ , $C_u = 10 \text{ kPa}$ $H/D = 1.67$
Geocell-reinforced granular base over clayey soil subgrade (G G C)	$\gamma_d = 23.1 \text{ kN/m}^3$ , $C_u = 10 \text{ kPa}$ $H/D = 1.67$ , $b/D = 4$ , $h/D = 1.33$ .
Geocell and basal geogrid-reinforced granular base over clayey soil subgrade (G BG G C)	$\gamma_d = 23.1 \text{ kN/m}^3$ , $C_u = 10 \text{ kPa}$ $H/D = 1.67$ , $b/D = 4$ , $h/D = 1.33$ , $B/D = 4.33$ .
Geocell-reinforced granular base over clayey soil subgrade and surface layer (G G C SL)	Surface layer $\gamma_d = 23.1 \text{ kN/m}^3$ , $C_u = 10 \text{ kPa}$ $H/D = 1.67$ , $b/D = 4$ , $h/D = 1.33$ .
Geocell and basal geogrid-reinforced granular base over clayey soil subgrade and surface layer (G BG G C SL)	Surface layer $\gamma_d = 23.1 \text{ kN/m}^3$ , $C_u = 10 \text{ kPa}$ $H/D = 1.67$ , $b/D = 4$ , $h/D = 1.33$ , $B/D = 4.33$

**Fig. 9.4** Typical loading pattern used in the test



computer-controlled servo-hydraulic actuator, with a maximum load of 9.7 kN and a minimum of 0.97 kN (10% of the maximum load) using a continuous haversine loading pattern as shown in Fig. 9.4 at a frequency of 1.0 Hz as described in Saride et al. (2013) to maintain a single-axle wheel load corresponding to a contact pressure of 550 kPa.

The depth of the reinforcement layer from the bottom of the plate was maintained at 0.1 times the diameter of the plate ( $u/D = 0.1$ ) according to Sitharam and Saride (2005) and Dash et al. (2003). The equivalent diameter of geocell pockets,  $d_c$ , was maintained at about  $1.6D$  in all the tests. Tests were terminated while reaching a plate settlement of about 20%.

## 9.4 Test Results

The data obtained from static and repeated load tests along with the instrumentation data are presented in terms of performance indicators. Influence of geocell, geocell with additional basal geogrid, geocell, and basal geogrid with flexible surface layer reinforcements on the performance improvement of weak clayey soil subgrades are presented. The performance improvement is quantified using several relevant parameters including improvement factors ( $I_f$ ), reduction in settlement (RS), especially from static load tests. The performance improvement due to repeated load tests is presented in terms of plastic deformations (PD), cumulative plastic deformations (CPD), which are also can be referred to as rut depth, and traffic benefit ratio (TBR), in addition to the elastic moduli viz apparent resilient modulus ( $M_r$ ), and modulus



improvement factor (MIF). The definitions of performance indicators are presented in the discussions.

### 9.4.1 Static Tests

Pressure-settlement responses were monitored to verify the performance of reinforced granular base layer overlying weak subgrade soil. The pressure-settlement responses observed for unreinforced and geocell-reinforced granular base test series are shown in Fig. 9.5. The stiffness of the granular base layers reinforced with different reinforcement forms viz geocell, geocell with additional basal geogrid with and without surface layer, has increased with amount and form of reinforcement. The load-bearing pressure of weak subgrade can be improved by placing a dense granular layer. It is noted that the load-bearing pressure of the weak subgrade has been increased by about two times with granular bases.

The improvement factor ( $I_f$ ), defined as the ratio of bearing pressure ( $q_c$ ) with geocell reinforcement at a given settlement to the corresponding pressure on unreinforced soil ( $q_o$ ) at the same settlement, is calculated for various reinforcement cases, and the variation of improvement factor for various test cases is presented in Fig. 9.6. The test configuration with geocell-reinforced granular base layer with basal geogrid and surface layer at 5% settlement ratio has obtained the maximum improvement factor of about 1.7. The geocell and basal geogrid provide lateral confinement and membrane support, respectively which is very important in any pavement section.

**Fig. 9.5** Variation of bearing pressure with settlement ratio for unreinforced and reinforced bases under static loading

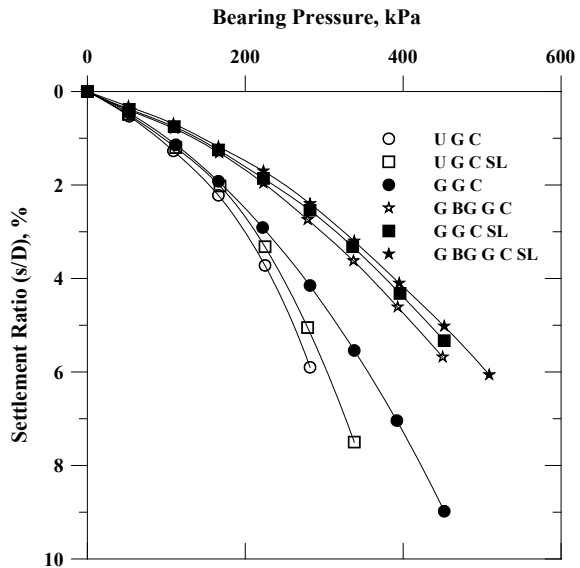
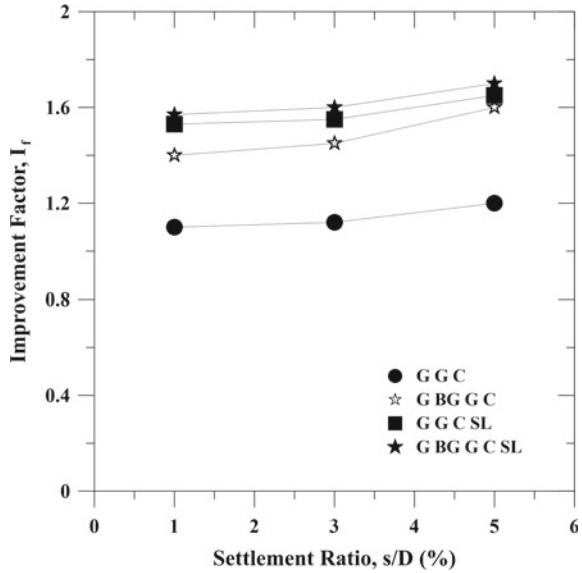


**Fig. 9.6** Variation of improvement factors with settlement ratio for reinforced bases



The percentage reduction in settlements (RS) is calculated at the loading plate settlements ( $s_r$ ) in the case of reinforced sand bed corresponding to the plate settlement ( $s_o$ ) of the unreinforced bed. The percentage reduction in settlement for granular bases is calculated for geocell, geocell with additional basal geogrid layer and surface layers, and the RS values are ranging between 30 and 60%. The maximum RS is obtained for the geocell and basal geogrid with surface layer case and minimum in the case of only geocell which is attributed to the decreased settlements corresponding to the ultimate bearing pressure of the unreinforced bed. The variation of the percent reduction in settlements is shown in Fig. 9.7 for different test configurations.

It is important to obtain the elastic modulus of unreinforced and reinforced granular base layers to visualize the contribution from reinforced base layer alone in the load-carrying mechanism. This information is crucial in obtaining the base layer thicknesses with and without geocell reinforcement using available elastic solutions for two-layer systems. The elastic modulus of unreinforced and reinforced beds, independent of the base material, using three well-known methods is calculated. The details of these well-versed methods are not discussed here. The elastic modulus obtained from each method is presented in Table 9.3. It can be seen that the Ueshita and Meyerhof (1967) and Burmister (1943) theories yielded similar results; however, the KENPAVE approach predicted slightly higher elastic modulus. The highest modulus of about 125 MPa was obtained in the case of geocell with a basal geogrid-reinforced granular base layer.

**Fig. 9.7** Variation of percent reduction in settlements, RS

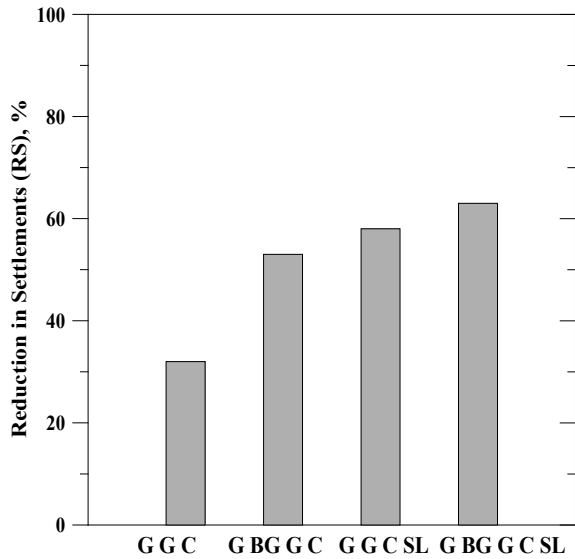


**Table 9.3** Modulus of base layer using different methods for various test cases

Method	Ueshita and Meyerhof (1967)	Burmister (1943)	Modulus improvement factor
Test case	$E_1$ (MPa)	$E_1$ (MPa)	$MIF = E_{1r}/E_{1u}$
U G C	49.6	49.5	—
G G C	82	81.8	1.65
G B G G C	117.6	117.5	2.4

### 9.4.2 Repeated Load Tests

Repeated load tests, as discussed in Sect. 9.2, were performed on the test configurations presented in Table 9.2. The data obtained from the repeated load tests along with the instrumentation data are presented in terms of performance indicators.

The performance improvement due to repeated load tests are presented in terms of cumulative plastic deformations (CPD), which also can be referred as rut depth, and traffic benefit ratio (TBR). The plastic/permanent deformations are cumulatively added to obtain the cumulative permanent deformations (CPDs) expressed in percentage of the plate diameter. Extension of the life of a pavement is defined in terms of traffic benefit ratio (TBR). TBR is defined as the ratio of the number of cycles necessary to reach a given rut depth for a test section containing reinforcement, divided by the number of cycles necessary to reach the same rut depth for an unreinforced section with the same section thickness and subgrade properties.

The pressure-settlement response of geocell with and without basal layer reinforced granular base course overlying weak subgrade under repeated loading is shown in Fig. 9.8. The total settlement ratio,  $s/D$ , defined as the ratio of plate settlement and the diameter of the plate, is higher for the initial loading cycles, while their magnitude attenuates with the number of repetitions. The geocell with basal layer-reinforced aggregate base sustained for higher repeated cycles due to higher frictional resistance of the aggregate material, which will provide higher interlocking and confinement, by the geocells and membrane effect by the basal layer (Fig. 9.8).

The pressure-settlement data is further analyzed to evaluate the permanent deformations (rutting) on the surface and elastic nature of the beds by separating the elastic and plastic components of the total plate settlement for each repetitive load cycle. The variation of plastic/permanent deformations with the number of load cycles for various cases of reinforced granular base layers overlying weak clayey subgrade is shown in Fig. 9.9. The permanent deformations are predominant in the initial cycles as can be witnessed from corresponding pressure-settlement curves (Fig. 9.8) and become almost minimal with an increase in the number of load repetitions. The highest permanent deformation for aggregate base, is about 3.0 mm for geocell alone case, and it has been reduced to 1.5 mm with the inclusion of basal geogrid (Fig. 9.9). This is due to the structural support provided by the geocell and the membrane support by the geogrid layer to the encapsulated base material within the geocell pockets.

Further, the permanent deformations are cumulatively added to obtain the cumulative permanent deformations (CPDs) expressed in percentage of the plate diameter. The variation of CPD's with the number of cycles is seen in Fig. 9.10. It is observed that the granular bases have sustained lower CPDs for a given number of load repetitions. The reduction in CPD's for reinforced cases is attributed to the increase in elastic response of the bed due to the reinforcement.

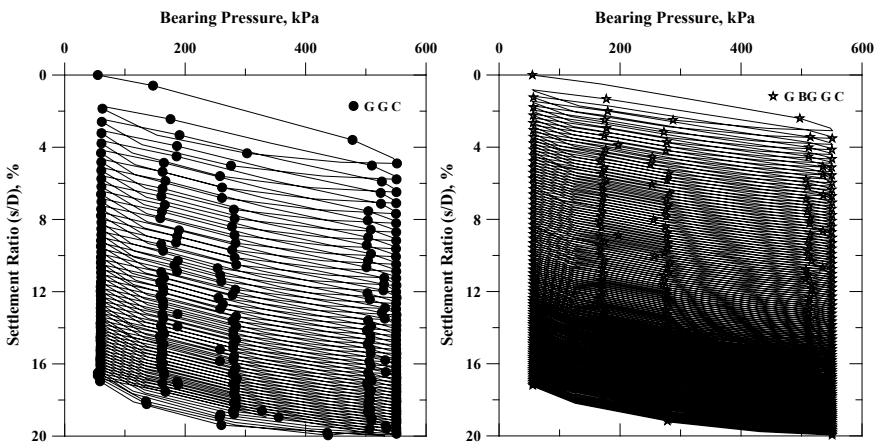


**Fig. 9.8** Variation of bearing pressure with settlement ratio for geocell, geocell with basal geogrid-reinforced granular base layer

**Fig. 9.9** Variation of permanent deformations with number of cycles for granular base layers

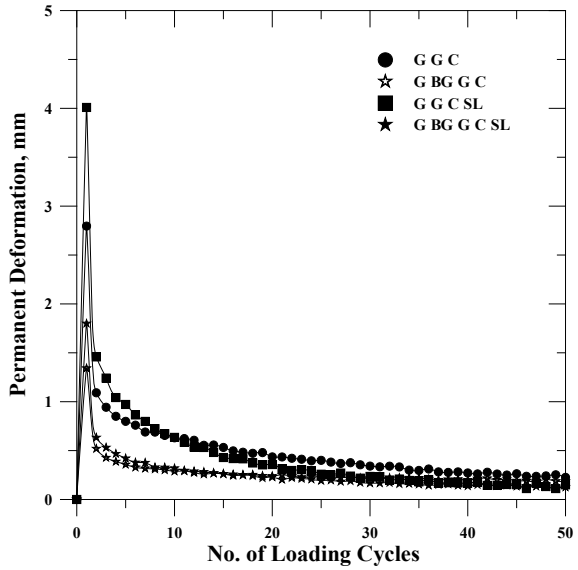
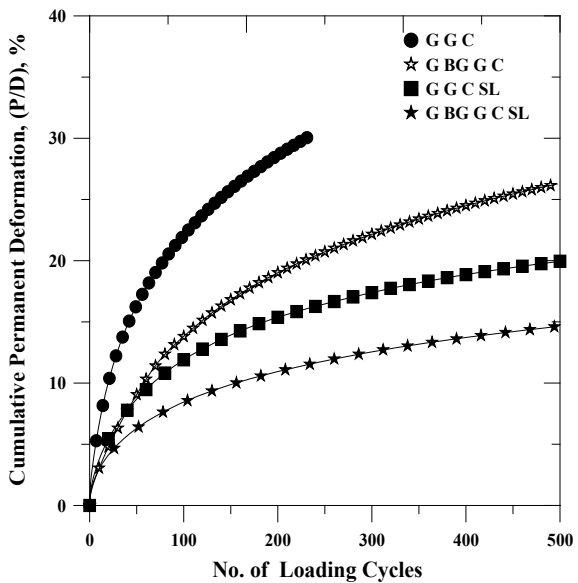
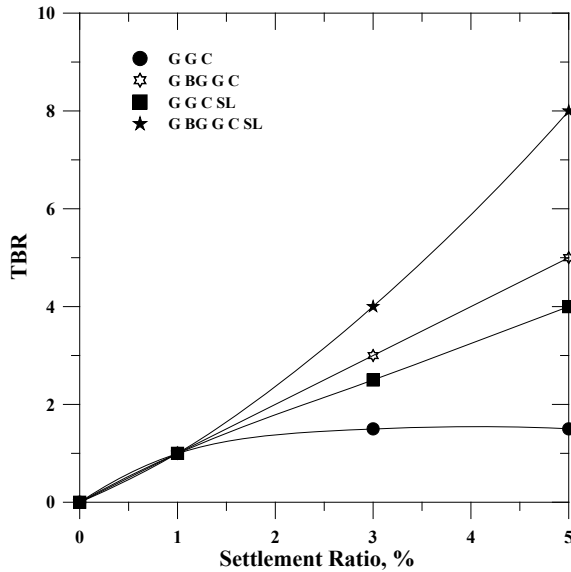


**Fig. 9.10** Variation of cumulative plastic deformations with number of cycles for granular bases



Further, the variation of TBR with the number of load repetitions is shown in Fig. 9.11. The traffic benefit with geocell reinforcement gradually increased with an increase in load repetitions. The case with geocell and geocell with basal geogrid-reinforced granular base layers resulted in a TBR of 1.5 and 5, respectively, at a 5% settlement ratio. The TBR further increased to 4 and 8 with the surface layer. The

**Fig. 9.11** Variation of TBR with settlement ratio for granular bases



higher TBRs are due to the combined membrane effect of the basal geogrid in addition to the confinement effect of the geocell and a stiff surface layer. Hence, for all practical purposes, the traffic benefit ratio shall be calculated when all the layers of flexible pavements are provided. The TBR values signify that the design life (or design traffic) of the pavement can be increased by about five times than its unreinforced section. In other words, the thickness of the pavement can be reduced with the optimal geocell configuration for a given design life of the pavement. Hence, base course thickness reduction can lead to economical pavement construction.

**Contact Stress Distribution**

The contact pressure on the weak subgrade was measured through several total earth pressure cells (TPC) placed at the interface as shown in Fig. 9.3. Figures 9.12, 9.13, and 9.14 present the surface deformations and contact stress distribution on the weak subgrade underlying unreinforced, geocell with/without basal geogrid-reinforced granular base layers with/without surface layer, respectively, under repeated single-axle traffic load conditions. The repeated load tests were conducted until the failure of the testbed. The contact pressure was recorded for each load cycle applied on the surface. The number of repetitive load cycles applied on the surface depends on the given configuration of the testbed. The contact pressure data is presented in terms of normalized contact pressure defined as a ratio of measured contact pressure on the weak subgrade to the applied contact tire pressure on the surface.

Figure 9.12 depicts the contact pressure distribution on the weak subgrade due to gradually increasing the cyclic load on the unreinforced granular base layer, as the unreinforced bed could not sustain at least a single repetitive load. Failure has occurred when the contact pressure reached about 400 kPa. At this pressure, the

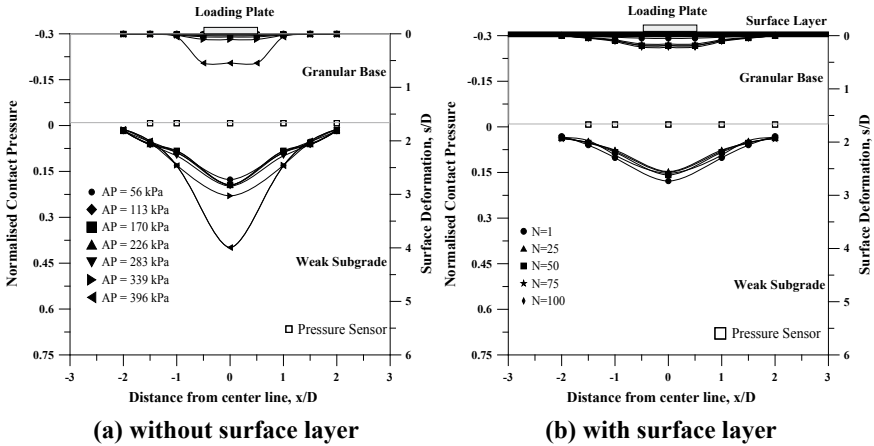


**Fig. 9.12** Surface deformation and contact pressure distribution on weak subgrade due to repeated load on unreinforced granular base layer

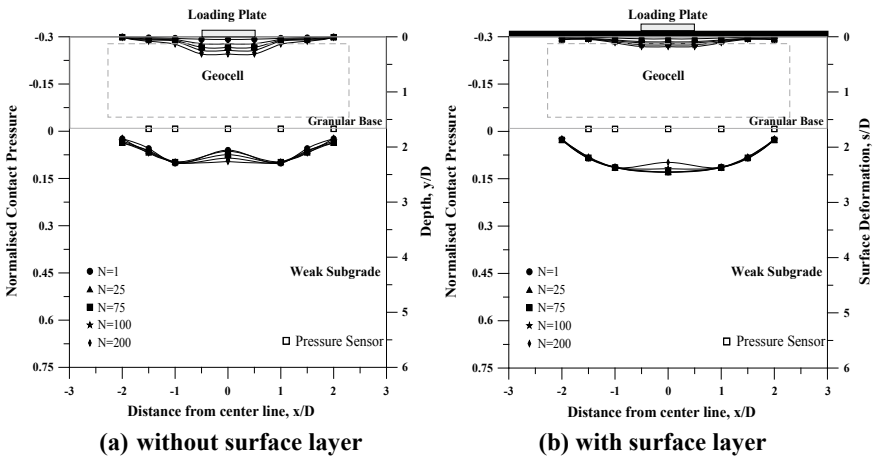


**Fig. 9.13** Surface deformation and contact pressure distribution on weak subgrade due to repeated load on geocell-reinforced granular base layer

contact pressure on the weak subgrade right underneath the loading area for the granular base is observed to be 145 kPa representing about 38% of the applied pressure. In other words, about 62% of the applied pressure has been absorbed by the granular base layer. It can also be seen that the pressure transmitted to the weak subgrade soil diminishes away from the loading region in the lateral direction. The contact pressure as low as about 1% of maximum applied pressure is recorded at a distance of  $2D$  and about 5% at  $1.5D$  from the centerline of the loading plate. Hence, the majority of the applied pressure has been transferred to the weak subgrade soil right underneath the

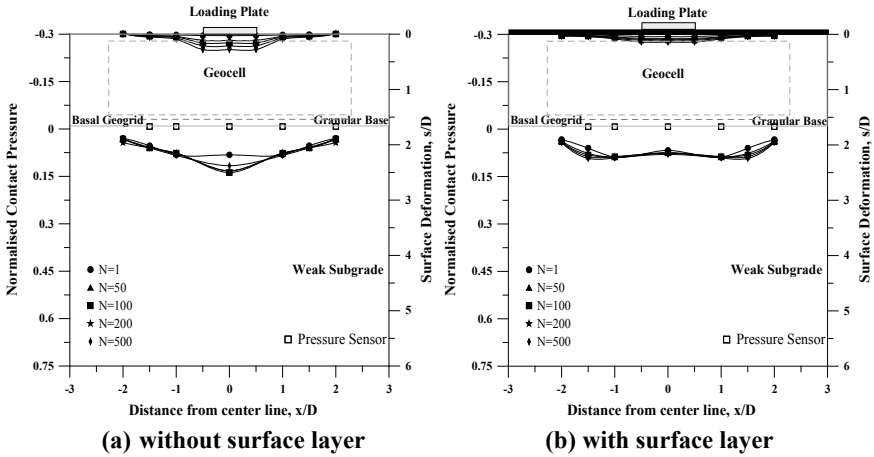


**Fig. 9.14** Surface deformation and contact pressure distribution on weak subgrade due to repeated load on geocell with basal geogrid-reinforced granular base layer

loading region leading to a low bearing pressure. With the surface layer on top, the contact pressures at the interface have drastically reduced.

The surface deformation at a maximum applied pressure of 400 kPa is 70 mm at the center underneath the loading region; however, the surface deformation is only 7 mm at the contact pressure of 340 kPa. With the surface layer, the surface deformations have reduced by about 70% even in the unreinforced test case. No heave is noticed on the surface.

With the inclusion of the geocell mattress of a predetermined size in the granular base layer, it has improved the performance of the bed (Fig. 9.13). Geocell reinforcement owing to its lateral confinement effect has improved the stiffness of the dense granular base layer. However, the test configuration has not sustained higher a number of repetitive load cycles owing to the interaction between the geocell and the granular base layer. However, a uniform contact pressure distribution is observed in this case. The normalized contact pressure is well within the range of 0.15. With the additional surface layer, the contact pressures have become more uniform under the loading region.

Figure 9.14 demonstrates that the geocell and basal geogrid reinforcement could enhance the performance of the granular base layer over weak subgrade under repetitive loading. Compared to the geocell-reinforced bed, geocell with basal geogrid-reinforced granular base performed well over the weak subgrade in terms of load repetitions before it has shown the failure. Geocell reinforcement owing to its lateral confinement and membrane effect of geogrid has improved the stiffness of the dense base layer. The surface layer could further reduce the contact pressure on the weak subgrade which can also be ascertained from the minimal surface deformations observed on the surface.



Further to the extensive laboratory study on the geocell-reinforced granular base layers, to establish the efficacy of the geocells in real field conditions, field trials were conducted.

## 9.5 Field Study

The field study was conducted on the Karnataka State Highway No 46 (KA SH 46), which mostly traverses through Ghats sections of the Dandeli reserve forest. The state highway is a two-lane road mostly on rolling terrain. The pavement section in the Dandeli forest area experienced severe rutting from heavy trailer traffic and weather conditions. Karnataka public works department (PWD) has proposed to rehabilitate these distressed roads. A trial section was given to experiment with geocell technology. It was proposed to use the granular sub-base (GSB) material as an infill for geocell mattress in place of conventional GSB base layers over an area of 8600 m<sup>2</sup> (about 1.5 km).

### 9.5.1 Construction of Test Sections

Two test sections viz unreinforced and geocell-reinforced (referred to as reinforced) GSB layers were built on SH 46 at Chainages 75 + 100 km and 75 + 110 km, respectively. At both locations, the existing pavement layers were completely removed up to the natural subgrade level. It was noticed that the existing road was built on a soling layer with a boulder-sized (300 mm) stones. The unreinforced section was constructed using a conventional GSB material alone. This section was used as a control section to compare the test data. In the case of the reinforced section, geocell was first stretched and filled with the GSB material. A typical schematic of the test sections (plan and sectional views) is shown in Fig. 9.15. A glimpse of the construction of test sections can be visualized in Fig. 9.16 in a sequence of plates.

#### Construction and Testing Sequence

- The existing pavement was scarified and removed with an excavator up to the subgrade level (Fig. 9.16a).
- Soling layer with boulder-sized stones was encountered and removed to the possible extent to reach the subgrade layer (Fig. 9.16a).
- Then, the subgrade was leveled and compacted using an 11.7-ton roller.
- A plate load test (PLT-1) was conducted on the subgrade.
- TPCs (#1, #2) were placed at predefined locations with utmost care to protect the cables.

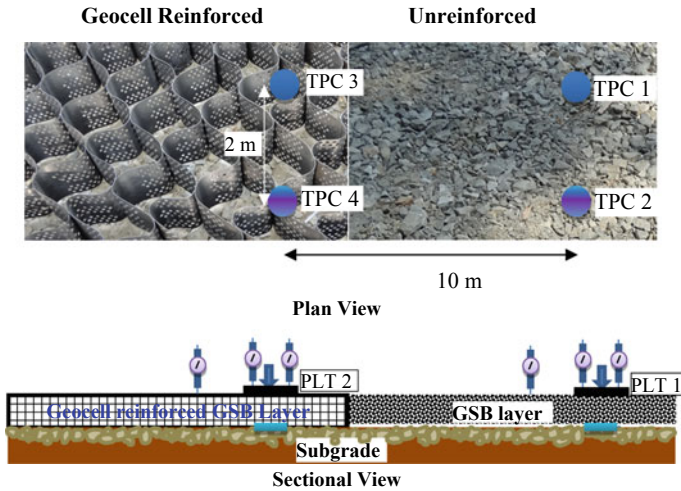


**Fig. 9.15** Plan and sectional views of the reinforced/unreinforced test sections

- A 150 mm thick and 10 m length GSB layer was placed, leveled, and compacted with the roller. Alternate roller passes were applied with a vibrating drum (Fig. 9.16b).
- In the case of geocell-reinforced section, after installing the TPCs (#3, #4), geocell mattress was spread on the subgrade. Then, the GSB material was spread in the geocell pockets (Fig. 9.16b).
- Then geocell-reinforced GSB layer of 150 mm and 10 m long section was built very adjacent to the unreinforced GSB section.
- Similar TPCs were used underneath the geocell-reinforced section (Fig. 9.16b).
- Cyclic plate load tests (PLT) were conducted, concentrically above the TPC nos. 2 and 4, again on both unreinforced and geocell-reinforced sections, respectively (Fig. 9.16c).
- Data from the near and farther TPCs were collected at each load increment.

### 9.5.2 Plate Load Tests

Slow cyclic plate load tests were conducted on the subgrade, unreinforced, and geocell-reinforced sections as per the procedure laid down in IS 1888-1982. A circular plate of size 300 mm diameter was selected to mimic the contact area of the vehicle's tire pressure. Two dial gauges were placed on the circular plate which was supported independently from an angular support system placed away from the loading area. Two dial gauges were used to monitor the fill surface movements. Since, one way of the road was operational and could not divert the traffic during testing, arranging a conventional type loading platform was replaced with a loaded multi-axel trailer



**a Excavation of existing pavement, preparation of site with instrumentation (TPCs)**



**b Instrumentation and construction of reinforced section**



**c Construction of geocell reinforced GSB layer and load test**

**Fig. 9.16** Construction sequence of unreinforced and reinforced pavement sections

weighing about 35 tons. Several other vehicles were tried prior such as a smooth drum roller of 11.7-ton capacity and a 20-ton capacity trailer. These relatively lighter vehicles were lifted off by the hydraulic jack system during the tests on subgrade soil itself, and hence, tests were repeated with a 35-ton multi-axel trailer with a full load. A typical arrangement of PLTs can be seen in Figs. 9.15 and 9.16. A hydraulic

jack of 30-ton with 150 mm travel was used to apply the load on to the plate against the reaction obtained from the trailer. The estimated ultimate load was applied in multiple increments, and the data from TPCs' dial gauges were collected at each load increment. The load on the circular plate was removed to zero levels at predetermined values. The settlement and elastic/plastic rebound of the plate were measured through dial gauges.

### ***9.5.3 Instrumentation and Data Collection***

The basic objective of instrumenting the test sections is to verify the total pressure distribution patterns beneath the unreinforced and geocell-reinforced layers. In each section, two total earth pressure cells (TPCs) were installed. These TPCs were spaced at a spacing of 2 m center to center [i.e., seven times the diameter of the plate approx. (7D)] and at a distance of 0.6 m from the edge of the pavement as shown in the schematic presented in Fig. 9.15. These locations are identified based on the estimation of the probable location of the wheel-base of most of the trailer traffic expected on the road. Four sensitive displacement dial gauges were used to measure the plate settlements and surface deformations. The TPC data was collected at every stage of the construction of test sections, roller compaction, etc., and during each load increment during the plate load tests.

### ***9.5.4 Results and Discussion***

#### **Pressure-Settlement Analysis**

The data from PLTs were analyzed, and load-settlement patterns were obtained for all the tests on the subgrade, unreinforced, and geocell-reinforced GSB sections. Figure 9.17 presents the monotonic load-settlement patterns of all the cases. It is imperative that the stiffness of the geocell-reinforced bed is higher than the unreinforced and subgrade alone sections. The subgrade section has shown an ultimate bearing pressure of about 800 kPa. The bearing pressure value is slightly higher for a silty clay type of soil subgrade. The higher bearing pressure of the subgrade may be attributed to the left-out portion of the soling layer in the subgrade. The unreinforced section has not shown a prominent failure due to the presence of the soling layer, however, the slope of the curve changed at about 17 mm of plate settlement. It is evident that the geocell-reinforced bed has not shown any clear marks of failure, but the bearing pressure has been linearly increasing with the plate settlement.

Figure 9.18 presents the cyclic behavior of unreinforced and geocell-reinforced GSB layers. The unreinforced sections did not sustain more than three cycles of the load against the geocell-reinforced section which was subjected to six cycles without a sign of failure even at 10% of the plate settlement. The initial elastic modulus calculated for each test case is presented in Table 9.4. It can be seen that the initial

**Fig. 9.17** Monotonic bearing pressure-settlement profiles

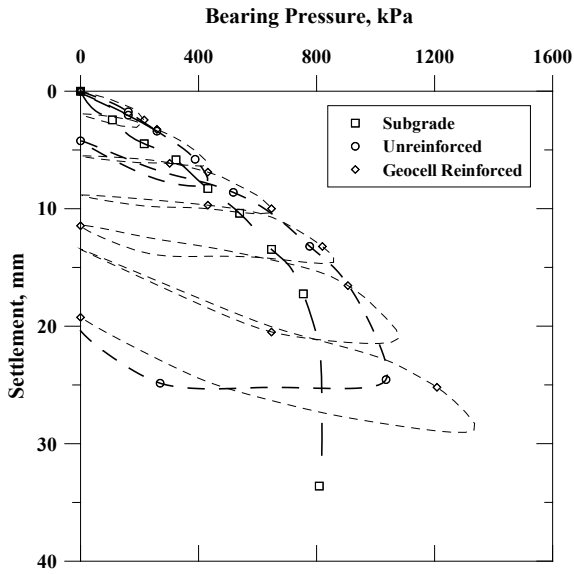
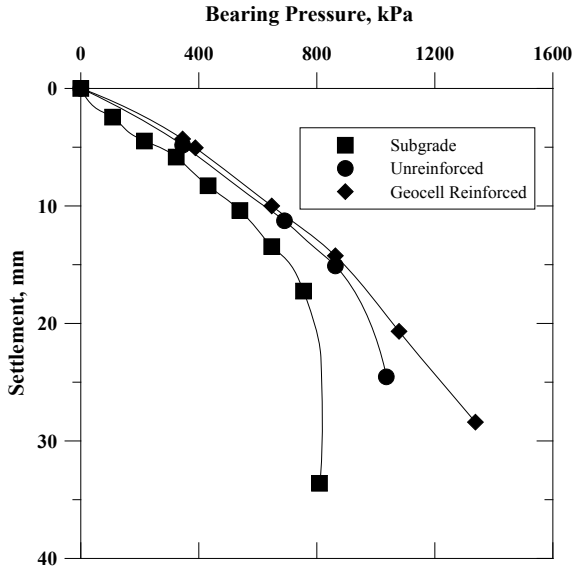


**Fig. 9.18** Bearing pressure-settlement profiles under cyclic loading

**Table 9.4** Properties of subgrade, GSB, and geocell-reinforced GSB materials

	$E_s$ , MPa <sup>a</sup>	$G$ , MPa <sup>a</sup>	$k_s$ , kN/m <sup>3</sup>	$M_r$ MPa	MIF
Subgrade	9.7	3.9	44,236	–	–
Unreinforced bed	24	9.4	106,798	29	–
Reinforced bed	32	12.7	143,821	69	2.35

Note <sup>a</sup>Calculations are done based on  $\mu = 0.25$ ;  $M_r$  = Resilient modulus, defined as the ratio of vertical stress to the elastic settlement

elastic modulus of the geocell-reinforced GSB is higher than the unreinforced bed owing to its higher confinement to the GSB materials which offers higher stiffness. The elastic modulus of subgrade, unreinforced, and reinforced beds are calculated by considering elastic rebound (settlement) from each cycle. It is apparent from Fig. 9.18 that the elastic component of the settlement of the unreinforced section is negligible in all the loading cycles. However, it can be seen that the elastic settlement of the geocell-reinforced section has increased with an increase in load due to the resilient response offered.

To quantify the efficacy of the geocell reinforcement further, deformation modulus values for each load cycle were calculated and presented in Fig. 9.20. The deformation modulus values were calculated from the initial tangent of each loading cycle. Besides, the deformation modulus was also calculated based on the German Institution of Standardization (DIN 18 2001) definition:

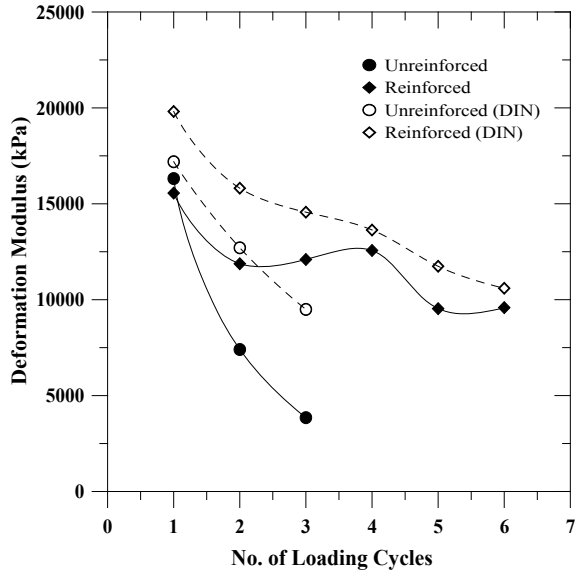
$$E_{\text{Def}} = 0.75 \times D \times \frac{\Delta\sigma}{\Delta s} \quad (9.3)$$

where  $D$  is the diameter of the plate and  $\Delta\sigma$  and  $\Delta s$  are the incremental stress and settlement under a load cycle.

Figure 9.19 presents the deformation modulus calculated from both the methods. In general, the deformation modulus decreases with an increase in loading cycles for both unreinforced and reinforced beds. After three load cycles to reach a bearing pressure of 700 kPa, the deformation modulus decreased for the geocell-reinforced GSB layer. This observation also confirms that the influence of the geocell is more exercised when the pressures are higher on the plate. Overall, it is inferred from these results that the geocell reinforcement improves the load-bearing pressure of the pavement layers by increasing the stiffness of the base course, reducing the permanent deformations, and by improving the deformation modulus of the system. In addition, the effectiveness of the geocell reinforcement can be experienced with higher initial compaction stresses on the infill (GSB) material.

Table 9.4 shows the elastic properties of all the test sections. The initial elastic modulus ( $E_s$ ), shear modulus ( $G$ ), and modulus of subgrade reaction ( $k_s$ ) have increased from subgrade case to geocell-reinforced GSB layer case. Besides, the geocell reinforcement has shown a higher resilient behavior than the unreinforced bed. However, at very high vertical stresses, the resilient modulus, defined as the ratio of vertical stress to the elastic settlement, of geocell-reinforced foundation bed

**Fig. 9.19** Variation of deformation modulus with number of load cycles



has reduced due to higher elastic strain. Table 9.4 shows the resilient modulus of reinforced and unreinforced beds at vertical stress of 400 kPa.

### 9.5.5 Pressure Distribution Beneath the Unreinforced/Reinforced GSB Layers

Total earth pressure cells (TPCs) of 3500 kPa capacity were installed beneath the unreinforced and geocell-reinforced GSB layers. The location of these TPCs can be visualized in Fig. 9.15 (sectional view). The plate load tests were conducted approximately concentrically on the TPC nos. 2 and 4 as shown in Fig. 9.15. The objective of this arrangement is to directly measure how much pressure is being transmitted to the bottom layers (subgrade). The other two TPCs were placed at about seven times the diameter of the plate (300 mm) which comes to about 2 m. These TPCs were embedded at a depth of 150 mm from the bottom of the plate. The TPCs were monitored for each load increment on the plate, and the results are presented in Figs. 9.20 and 9.21. Figure 9.20 shows the pressure distribution beneath the unreinforced bed from TPCs 1 and 2. It is clearly seen that the TPC2 has experienced about 66% of the applied pressure on the plate. The pressures recorded at TPC1 is almost negligible in the pressure range applied to elucidate that the GSB layer is more discrete and distributed the pressure directly to the subgrade without spreading. On the contrary, the TPCs placed under the geocell-reinforced GSB layer have experienced much lesser pressure even at very high pressures on the plate. The applied pressure transmitted to the subgrade accounts to about only 16% of the total

**Fig. 9.20** Pressure distribution below the unreinforced GSB layer

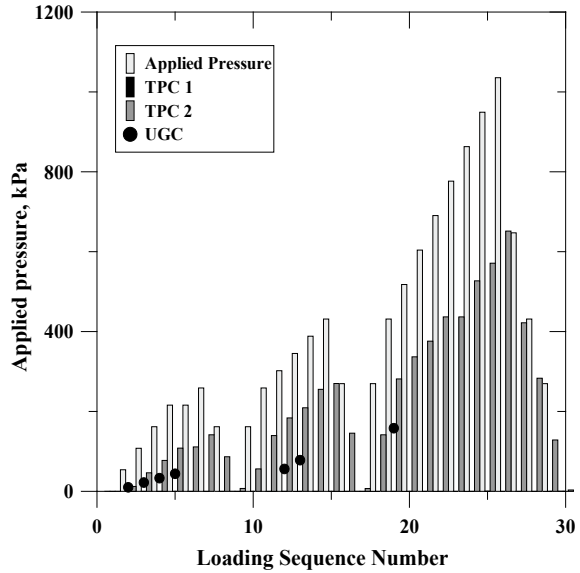
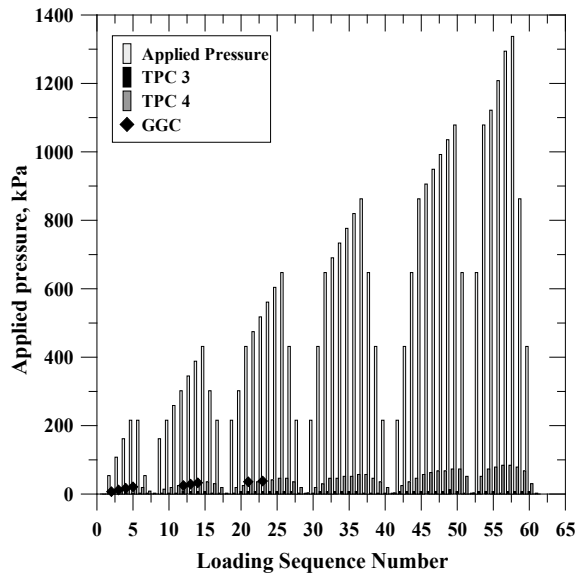


**Fig. 9.21** Pressure distribution below the geocell-reinforced GSB layer



applied pressure on the plate. The reinforced bed has distributed the applied pressure to a larger area, where the TPC3 placed at a distance of 7D has experienced about 12% of the pressure transmitted under the area of loading (at TPC4). It is interesting to note that the influence of the geocell mattress is better drawn for higher load applications. This can be illustrated that the pressure transmitted to the subgrade is



only 5.8% at the maximum pressure (~1000 kPa) on the plate. This confirms that the geocell reinforcement is redistributing the applied pressure transmitting to a wider area around the loading region. This higher pressure re-distribution would have taken place up to a distance of about  $5D$  from the centerline of the loading plate.

Figure 9.21 also depicts the contact pressure measured in the laboratory experiments for similar test cases (refer Figs. 9.12a and 9.13a) under similar loading conditions. It is interesting to see that the field and laboratory observations are closely matching. Small deviations observed can be attributed to the prevailing subgrade conditions. In the case of laboratory tests, the subgrade is softer than the field situation.

Overall, the performance of the granular base layers in terms of an increase in load-carrying capacity and reduction in rutting and contact pressure over the weak subgrades can be improved through geocell reinforcement. The resilient modulus and modulus improvement factors obtained from both laboratory and field studies are in concurrence, and these parameters will be very vital in designing the pavements with geocell reinforcement.

## 9.6 Design of Geocell-Reinforced Pavements

The Indian roads congress (IRC) and Ministry of Road Transport and Highways (MoRTH) approved the use of geosynthetics in highway construction. Guidelines for using geosynthetics in road pavements were issued by IRC (2019) and MoRTH (Section 700) (Ministry of Road Transport & Highways 2013). Currently, IRC (2019) has incorporated geogrids and geocells in road pavement construction. The IRC SP 59 (2019) uses the following design methodologies to incorporate geogrids and geocells in the pavement construction.

### 9.6.1 *Traffic Benefit Ratio (TBR) Based Design*

To design a pavement with geocell reinforcement, the TBR approach can be adopted either to reduce the thickness of the base course or to increase the service life of the pavement. In brief, to design an unreinforced pavement section, according to the American Association of State Highways and Transportation Officials (AASHTO), flexible pavement's overall structural number (SN) needs to be calculated (AASHTO 1993). In order to design the geocell-reinforced pavement, TBR is used. The effect of geocell reinforcement is quantified in terms of equivalent structural number by considering traffic to be catered by the pavement and TBR that can be obtained with selected geocell. The equivalent structural number of geocell is then used to reduce the unreinforced pavement base layer thickness to the extent of the reinforcement effect. A step by step procedure to design geocell-reinforced pavement using TBR approach is as follows:

- Step 1. Design the unreinforced pavement by considering subgrade soil CBR or resilient modulus and the traffic to be catered as per the guidelines provided by IRC 37 (2012).
- Step 2. Compute the total structural number ( $SN_{UR}$ ) of the unreinforced pavement structure designed in Step 1 taking into account the appropriate layer coefficients and drainage coefficients and thickness of each layer per AASHTO (1993) using Eq. 9.4.

$$SN_{UR} = a_1 D_1 + a_2 D_2 m_2 + a_3 D_3 m_3 \quad (9.4)$$

- Step 3. Compute the  $SN_{req}$  required over the subgrade of unreinforced pavement to cater the design traffic (number of standard axle load passes,  $W_{18UR}$ ) using the following equation and substituting the appropriate values in Eq. 9.5.

$$\log(W_{18}) = Z_R S_0 + 9.36 \log_{10}(SN + 1) - 0.2 + \frac{\log_{10} \left[ \frac{\Delta PSI}{4.2 - 1.5} \right]}{0.4 + \frac{1094}{(SN+1)^{5.19}}} + 2.32 \log_{10} M_R - 8.02 \quad (9.5)$$

- Step 4. Select an appropriate traffic benefit ratio (TBR) based on full-scale field studies or large-scale laboratory studies that represent similar field conditions and failure criteria. TBR typically ranges from 2 to 6 depending on the stiffness of the geocell/geogrid, subgrade CBR, base/sub-base thickness, and asphalt concrete layer thickness.
- Step 5. Compute the number of standard axle load passes,  $W_{18R}$ , that can be allowed on the reinforced pavement structure by multiplying TBR with  $W_{18UR}$ .
- Step 6. Compute the structural number,  $SN_R$ , of pavement which can cater computed number of standard axle passes,  $W_{18R}$ , with reinforcement using Eq. 9.5.
- Step 7. Find the equivalent structural number of geocell by subtracting  $SN_{UR}$  from  $SN_R$ .
- Step 8. Reduce the base/sub-base layer thickness taking into account the equivalent structural number of geocell meeting the minimum base/sub-base layer thickness criteria and total structural number ( $SN$ ) of unreinforced pavement.

### Example: Design of reinforced flexible pavements using TBR approach

Consider designing a pavement section on a weak subgrade CBR of 3% and for design traffic of 50 msa.

#### Design Steps:

- Obtain the unreinforced pavement layer thicknesses as per IRC: 37 (2012):  
 Combined bituminous layers = 190 mm  
 Granular base and sub-base layers = 600 mm

- Compute the Structural Number (SN) =  $a_1 * D_1 + a_2 * D_2 * m_2 + a_3 * D_3 * m_3$   
 Compute resilient moduli of pavement layers:  
 From IRC 37-2012,  $M_{R\text{Bitumen mix}} = 3000 \text{ MPa} = 435,113 \text{ psi}$   
 $a_1 = 0.171 (\ln (M_{R\text{Bitumen mix}})) - 1.784 = 0.436/\text{in.} = \mathbf{0.0172/\text{mm}}$   
 From IRC 37-2012, for base  $M_{R\text{gb}} = 0.2 * M_{R\text{gsb}} * h^{0.45}$   
 $M_{R\text{gb}} = 0.2 * 84 * 250^{0.45} = 200.95 \text{ MPa} = 29,145 \text{ psi}$   
 $a_2 = 0.249(\log_{10} (M_{R\text{gb}})) - 0.977 = 0.135/\text{in.} = \mathbf{0.0053/\text{mm}}$   
 Form IRC 37-2012 for sub-base  $M_{R\text{gsb}} = 0.2 * M_{R\text{subgrade}} * h^{0.45}$   
 $M_{R\text{subgrade}} = 10 * \text{CBR MPa} = 30 \text{ MPa}$   
 $M_{R\text{gsb}} = 0.2 * 30 * 350^{0.45} = 84 \text{ MPa} = 12,147 \text{ psi}$   
 $a_3 = 0.227(\log_{10} (M_{R\text{gsb}})) - 0.839 = 0.0918/\text{in.} = \mathbf{0.0035/\text{mm}}$   
 Let drainage coefficients  $m_2$  and  $m_3$  be 1.00 and 1.00 for WMM and GSB  
 $\text{SN} = 0.0172 * (190) + 0.0053 * 250 * 1.0 + 0.0035 * 350 * 1.0$   
 $\text{SN}_{\text{UR}} = 5.803$
- Now, compute the required structural number:

$$\log(W_{18}) = Z_R S_0 + 9.36 \log_{10}(\text{SN} + 1) - 0.2 + \frac{\log_{10} \left[ \frac{\Delta \text{PSI}}{4.2 - 1.5} \right]}{0.4 + \frac{1094}{(\text{SN} + 1)^{5.19}}} + 2.32 \log_{10} M_R - 8.02$$

$W_{18 \text{ Unreinforced}} = 50 \text{ MSA}$

$Z_R = -1.282$  (for 90% reliability)

$S_0 = 0.4$  (overall standard deviation for flexible pavement)

Change in pavement serviceability index (PSI) = Initial PSI—terminal PSI

$\Delta \text{PSI} = p_0 - p_t = 4.3 - 2.0 = 2.3$

$M_R = 4351 \text{ PSI} = 30 \text{ MPa}$  ( $3 * 10$  for 3% CBR subgrade soil)

**$\text{SN}_{\text{Req}} = 6.521$**

- **Computation of  $\text{SN}_R$**

Let  $TBR$  be 3.0

$W_{18 \text{ Reinforced}} = 50 * 3 = 150 \text{ msa}$

$$150 \text{ msa} = Z_R S_0 + 9.36 \log_{10}(\text{SN} + 1) - 0.2 + \frac{\log_{10} \left[ \frac{\Delta \text{PSI}}{4.2 - 1.5} \right]}{0.4 + \frac{1094}{(\text{SN} + 1)^{5.19}}} + 2.32 \log_{10} M_R - 8.02.$$

**$\therefore \text{SN}_R = 7.469$**

- Equivalent structural number of geocell =  $\text{SN}_R - \text{SN}_{\text{Req}} = 7.469 - 6.521 = 0.948$
- Reduce base layer thicknesses of geocell-reinforced pavement after considering the equivalent structural number of geocell:  
 Adjust the thicknesses of pavement layers to yield an  $\text{SN} \geq 4.855$  ( $5.803 - 0.948$ ).  
 Maintain a minimum base thickness of 150 mm (IRC 37 2012).

**Trial 1: Let the reduced thickness of GSB be 210 mm**

$\text{SN} = a_1 * D_1 + a_2 * D_2 * m_2 + a_3 * D_3 * m_3$

$\text{SN} = 0.0172 * 190 + 0.0047 * 250 * 1.0 + 0.0032 * 210 * 1.00 = \mathbf{4.947} > \mathbf{4.855}$

( $a_2, a_3$  are computed based on the reduced thickness).

The reduced thickness of the GSB layer satisfies the structural number required. Hence, the pavement is safe against the fatigue and rutting strains (which can be verified by the IITPAVE program) for the reduced pavement thickness. In this analysis, the geocell reinforcement could reduce a combined base/sub-base course thickness from 600 to 360 mm, which is about a 40% reduction in granular layers.

### 9.6.2 Layer Coefficient Ratio (LCR) Based Design

The layer coefficient represents the improvement in the strength of the pavement layer. It can be estimated based on the modulus improvement factor (MIF) (Giroud and Han 2013) as shown below.

$$\text{LCR} = \frac{0.249 \log 10\left(\text{MIF} * \frac{\text{Mrbc}}{0.0069}\right) - 0.977}{0.249 \log 10\left(\frac{\text{Mrbc}}{0.0069}\right) - 0.977} \quad (9.6)$$

where

$M_{\text{rbc}}$  = Resilient modulus of base course

MIF = Modulus improvement factor.

The resilient modulus of the base layer ( $M_{\text{rbc}}$ ) can be obtained from Eq. 9.7 presented in IRC-37 (2012). The modulus may also be obtained from the resilient modulus test obtained using a cyclic triaxial test on the material. Eq. 9.7 may be used to calculate the  $MR_{\text{bc}}$ .

$$M_{\text{rbc}}(\text{MPa}) = 29.4(\text{CBR})_{\text{bc}}^{0.4358} \quad (9.7)$$

where  $\text{CBR}_{\text{bc}}$  = CBR value of the base course in percentage.

Modulus improvement factor (MIF) is a ratio of elastic modulus of the upper reinforced base layer ( $E_{1\text{R}}$ ) to the elastic modulus of the unreinforced bed ( $E_{1\text{U}}$ ) with the same test configuration.

$$\text{MIF} = \frac{E_{1\text{R}}}{E_{1\text{U}}} \quad (9.8)$$

where

$E_1$  = Elastic modulus of the base layer with and without geocell reinforcement.

These values under laboratory and field test conditions can be seen in Tables 9.3 and 9.4, respectively. Based on the MIF values, the layer coefficient ratio (LCR) of the geocell-reinforced base layers may vary between 1.2 and 1.7. Beyond this range, the pavements may become unsafe either in fatigue or rutting, or uneconomical.

## 9.7 Conclusions

1. Geocell can be effectively used as a reinforcement system in pavement base/sub-base layers to increase the stiffness and resilient behavior.
2. The provision of additional basal geogrid to the geocell reinforcement resulted in a reduction of 75% in permanent settlements.
3. The elastic modulus of the geocell-reinforced aggregate base with an additional basal layer is found to be 125 MPa against a modulus of 4.4 MPa for unreinforced bed.
4. The apparent resilient modulus from the cyclic load tests on geocell-reinforced aggregate base with additional basal layer is found to be 65 MPa against 20 MPa for unreinforced bed.
5. As high as 86% reduction of contact pressure on the clayey soil subgrade is obtained. It has been noticed that the distribution of pressures is uniform over a wider area in the case of geocell and geogrid-reinforced dense granular base layers with a surface layer in cyclic load tests.
6. Geocell and basal geogrid with surface layer reinforcement reduce the plastic settlements by about eight and elastic settlements by twofolds, referred to as rutting and resilient behavior on the pavement surface by providing lateral confinement from the geocell and membrane support from geogrid and surface layer to the infill soil.
7. A CPD reduction of almost five and sevenfold against geocell-reinforced alone is observed. The reduction in CPD's for reinforced cases is attributed to the increase in elastic response of the bed.
8. Traffic benefit ratio (TBR) calculated at 5% of the loading plate settlement has increased with reinforced test cases. A TBR of as high as eight is observed in the case of geocell with basal geogrid-reinforced granular bases with a surface layer. The modulus improvement factors are observed to be about 2.5 based on both laboratory and field studies.
9. Geocell reinforcement owing to its lateral confinement has improved the stiffness of the dense granular base layer. A fairly uniform contact pressure distribution is observed. The normalized contact pressure at the interface of the granular base and weak subgrade layers is observed to be well within the range of 0.15.
10. It can be observed that about 62% of the applied pressure has been absorbed by the granular base layer and transmitted about 38% to the underlying weak subgrade layer.
11. The deformation modulus seems to reduce with an increase in reinforcement form in the base layer.
12. Two design methodologies viz traffic benefit ratio approach, and layer coefficient ratio approach are discussed.

## References

- AASHTO (1993) Guide for design of pavement structures. American Association of State Highway and Transportation Officials, Washington, DC
- AASHTO (2009) Standard practice for geosynthetic reinforcement of the aggregate base course of flexible pavement structures. American Association of State Highway and Transportation Officials (AASHTO), R 50-09, Washington, DC
- Barke WR (1987) Open-graded bases for airfield pavements, Technical Report GL-87-16, USAE Waterways Experiment Station, Vicksburg, MS, USA, 76 p
- Barksdale RD, Brown SF, Chan F (1989) Potential benefits of geosynthetics in flexible pavement systems, National Cooperative Highway Research Program Report No. 315, Transportation Research Board, National Research Council, Washington, DC
- Burmister DM (1943) The theory of stresses and displacements in layered systems and applications to the design of airport runways. In: Proceedings of the 23rd Annual Meeting of the Highway Research Board, pp 126–148
- Chummar AV (1972) Bearing capacity theory from experimental results. *J of the Geotech Engg*, ASCE 98(12):1311–1324
- Collin JG, Kinney TC, Fu X (1996) Full scale highway load test of flexible pavement systems with geogrid reinforced base courses. In: *Geosynthetics Intentional*, Industrial Fabrics Association International, Roseville, MN, 3(4):537–549
- Dash SK, Saride S, Sitharam TG (2003) Model studies on circular footing supported on geocell reinforced sand underlain by soft clay. *Geotext Geomembr* 21(4):197–219
- DIN 18 134 (2001) Determining the deformation and strength characteristics of soil by the plate loading test. German Standards
- Giroud JP, Han J (2013) Design of geosynthetic-reinforced unpaved and paved roads. Short course, *Geosynthetics 2013*, Long Beach, CA, April 4
- Haas R, Wall J, Carroll RG (1988) Geogrid reinforcement of granular bases in flexible pavements. In: *Transportation Research Record 1188*, TRB, National Research Council, Washington, DC, USA, pp 19–27
- IRC SP 59 (2019) Guidelines for use of geotextiles in road pavements and associated works, First revision, Indian Roads Congress, New Delhi
- IRC: 37-(2012) Guidelines for the design of flexible pavements (3rd Revision)
- Latha GM, Nair AM, Hemalatha MS (2010) Performance of geosynthetics in unpaved roads. *Int J Geotech Eng* 4(2):151–164
- Ministry of Road Transport & Highways (2013) Specifications for road and bridge works, Section 700, 5th revision
- Perkins SW, Ismeik MA (1997) Synthesis and evaluation of geosynthetic-reinforced base course layers in flexible pavements: part i experimental work. *Geosynthetics Int* 4(6):549–604
- Pokharel SK (2010) Experimental study on geocell-reinforced bases under static and dynamic loading. D Phil Thesis, University of Kansas, USA
- Pokharel SK, Han J, Manandhar C, Yang X, Leshchinsky D, Halahmi I, Parsons RL (2011) Accelerated pavement testing of geocell-reinforced unpaved roads over weak subgrade. *Transp Res Rec* 2204:67–75
- Rajagopal K, Veeraragavan A, Chandramouli S (2012) Studies on geocell reinforced road pavement structures. *Geosynthetics Asia 2012*, Thailand
- Saride S, Rayabharapu VK, Suraj V, Anand JP (2013) Repeated load tests on geocell reinforced sand subgrades. In: Proceedings of the geosynthetics international conference, Long Beach, CA, 3(4):537–549
- Saride S, Rayabharapu VK, Suraj V (2015) Evaluation of rutting behavior of geocell reinforced sand subgrades under cyclic loading. *Indian Geotech J* 45(4):378–388
- Sitharam TG, Saride S (2005) Behaviour of embedded footings supported on geocell reinforced foundation beds. *ASTM Geotech Test J* 28(5):452–463

Ueshita K, Meyerhof GG (1967) Deflection of multilayer soil systems. J Soil Mech Found Div ASCE SM5:257-282